Light-gradient Mixing Performance Improvement of the Flat Plate Photobioreactor with Waved Baffles

L. Wang and X. You*
School of Environmental Science and Engineering
Tianjin University, Tianjin 300072, China

Original scientific paper
Received: May 29, 2012
Accepted: December 5, 2012

A computational fluid dynamics (CFD) simulation of a flat plate photobioreactor with waved baffles was performed. The research of the ratio of waved baffle height to wave length (L/λ) and the ratio of wave amplitude to wave length (A/λ) on light-gradient mixing was made. The optimized waved baffles structures of L/λ=12 and A/λ=0.2 was obtained, under which both the average turbulent kinetic energy in the downcomer ($(TKE)_d$) and average liquid radial velocity in the downcomer (U_d) were larger. The light-gradient mixing was enhanced. Through the performance evaluation, $(TKE)_d$ increased about 35 % under the action of the optimized waved baffles than under traditional flat baffles. The statistical analysis method was employed, which reflects the light-gradient mixing more precisely than mean value. It is shown that the proportion of negative velocities indicating the radial mixing condition was 2.5 times larger in the optimized waved baffles than in traditional flat baffles.

Key words:
CFD; Photobioreactors; Waved baffles; Mixing;

Introduction

Microalgae synthesizes many highly valuable products such as protein, carbohydrate, astaxanthin and other bioactive compounds .[1] It has been widely used in the food industry, waste treatment, aquaculture and biofuel production .[2–4] High-density culture process is of primary interest. The open pond and closed photobioreactor (PBR) are widely used in microalgae culture.[5,6] It was shown that closed PBR had better performance than that of raceway ponds in culture condition and microalgae production.[7] However, many problems such as technical expenses, light utilization and production scale-up are left for the development and application of PBR.[8–10] The market of industrial microalgae production is still small because of the backward photobioreactor technology and economic challenges.[10,11] Therefore, the development of new PBR with high cultivation efficiency and low costs is becoming an important task in applying microalgal biotechnology.

Light is a critical factor for microalgal growth and the accumulation of valuable metabolites.[12] For a PBR, besides a good flow field condition and mass transfer performance, the light energy utilization efficiency also needs to be enhanced. Richmond[13] found the mixing was the most practical way to distribute radiation evenly to all cells, as well as to accelerate microalgal growth by reducing the diffusion barriers around the cells. Perner-Nachta et al.[14] investigated the light intensity variation in a tubular photobioreactor with helical static mixers which have the potential of improving radial flow. Su et al.[15] made a study on the destabilization mixing in a flat plate photobioreactor by means of using the destabilizing bar which can effectively intensify mixing along the light gradient. Yu et al.[16] assumed the mixing condition, especially mixing in the irradiance direction, affected algal growth directly. They found that the better the mixing in the irradiance direction the larger the microalgae production. Therefore, good mixing performance along with the irradiance direction is required when the PBR is optimized.

The guide plate in airlift PBR promotes the process of gas-liquid mass transfer and mixing.[15,17] However, former studies always focused on the smooth cylinder and flat plate type. According to the study of Li,[18] waved baffles perform well in flow field and mass transfer process. In addition, the optimal structure parameters of the whole PBR were found. Unfortunately, their study lacked systematic research into the structure of waved baffles, as well as the mixing characteristic in the irradiance direction.

This paper establishes a three-dimensional computational fluid dynamics (CFD) model of a flat PBR with waved baffles. The simulation was performed with a two-fluid model. After confirming the reliability of the simulation, the structure

*Corresponding author: Xue-yi You; tel: +86-22-27403561; fax: +86-22-27403561; email: xyyou@tju.edu.cn

parameters of the waved baffles, i.e. the ratio of waved baffle height to wave length (L/λ) and the ratio of wave amplitude to wave length (A/λ), were taken to analyze their mechanism on the light-gradient mixing performance. The optimized structure of waved baffles, which heped to enhance the light-gradient mixing performance was obtained. It is shown that the waved baffles have great potential to be used in the design of bioreactor and PBR.

Materials and methods

Reactor configuration

The airlift PBR with waved baffles used by Li[18] was chosen here. The schematic diagram of the PBR and the waved baffle are shown in Fig. 1 (a). L represents the waved baffle height, *h* is the central axis of the waved baffle, A and λ represent wave amplitude and wave length, respectively. The dimensions of PBR are 400 mm in length (z-axis), 80 mm in width (x-axis) and 500 mm in height (y-axis). The reactor was initially filled with water to a height of 400 mm and the liquid volume was 12.8L. Air was injected into the reactor through a perforated plastic tube with diameter of 6.5 mm. The plastic tube was pointed at the same height with the bottom of the waved baffle. The air-inlet plastic tube contained 38 holes with diameter of 0.5 mm and the holes were 1 cm apart. The ratio of the cross-section area of the downcomer (A_d) to that of the riser (A_T) was 1.05 (A_d/A_T=1.05). The clearance from the upper edge of the waved baffles to the water level (a) was a=60 mmand the clearance from the lower edge of the waved baffles to the bottom of the reactor (b) was b=60mm.

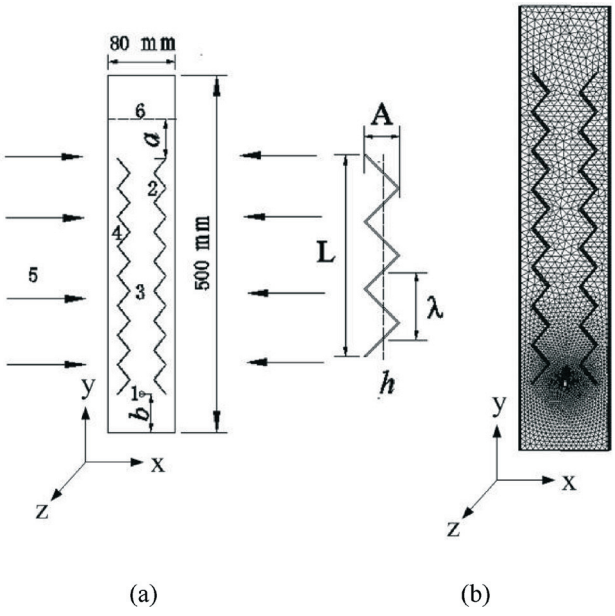

(a) (b)

Fig. 1 – *Schematic diagrams of a flat plate PBR with waved baffles (a) and its mesh for CFD simulation (b) 1. Gas sparger 2. Waved baffles 3. Riser 4. Downcomer 5. Light illumination 6. Water level*

Methodology for computational fluid dynamics

Euler-Euler model was applied to describe the gas-liquid flow. The model assumes that the two phases are interpenetrating and incompressible. The flow was isothermal and isotropic turbulence assumption was used.

The conservation equations of mass and momentum were as follows:

Continuity equations of continuous (q) and dispersed (p) phase

$$\frac{\partial}{\partial t}(\alpha_q \rho_q) + \nabla \cdot (\alpha_q \rho_q \vec{v}_q) = 0 \quad (1)$$

$$\frac{\partial}{\partial t}(\alpha_p \rho_p) + \nabla \cdot (\alpha_p \rho_p \vec{v}_p) = 0 \quad (2)$$

Momentum equations of phase

$$\frac{\partial}{\partial t}(\alpha_q \rho_q \vec{v}_q) + \nabla \cdot (\alpha_q \rho_q \vec{v}_q \vec{v}_q) = -\alpha_q \nabla p + \nabla \cdot \bar{\bar{\tau}}_q + K_{pq}(\vec{v}_q - \vec{v}_p) - m_{pq}\vec{v}_{pq} + m_p \rho_p g + \alpha_p \rho_p \bar{F} \quad (3)$$

$$\frac{\partial}{\partial t}(\alpha_p \rho_p \vec{v}_p) + \nabla \cdot (\alpha_p \rho_p \vec{v}_p \vec{v}_p) = -\alpha_p \nabla p + \nabla \cdot \bar{\bar{\tau}}_p + K_{pq}(\vec{v}_q - \vec{v}_p) - m_{pq}\vec{v}_{pq} + m_p \rho_p g + \alpha_p \rho_p \bar{F} \quad (4)$$

$\bar{F}$ represents the interphase force such as drag, lift, virtual mass and so on. Many authors found that the virtual mass force and lift force had no significant effects on the gas-liquid flow in the airlift bioreactor.[19,20] In the former studies, only drag force was considered in simulation because of the low gas flow velocity and gas holdup calculated from Li's study.[18] The drag force on a single bubble in the direction of coordinate i is expressed as:

$$F_{i,q} = -F_{i,p} = \frac{3}{4}\alpha_q \alpha_p \rho_q \frac{C_D}{d}|\vec{v}_p - \vec{v}_q|(\vec{v}_{i,p} - \vec{v}_{i,q}) \quad (5)$$

When the bubble diameter is small such as the case in this approach, the changes of drag force by different drag laws are small[20] and there is no significant effect on the gas-liquid flow.[21] Therefore, the drag coefficient C_D was calculated by[22]

$$C_D = \begin{cases} \frac{24}{\mathrm{Re}}(1 + 0.15\,\mathrm{Re}^{0.687}) & \text{if } \mathrm{Re} < 1000 \\ 0.44 & \text{if } \mathrm{Re} \geq 1000 \end{cases} \quad (6)$$

Where the Reynolds number was defined as

$$\mathrm{Re} = \frac{\rho_q |\vec{v}_p - \vec{v}_q| d}{\mu_q} \quad (7)$$

The standard *k-ε* model was used to model the turbulence of continuous phase. The turbulent viscosity in the continuous phase is

$$\mu_{t,q} = C_\mu \rho_q k_q^2 / \varepsilon_q \tag{8}$$

The turbulent kinetic energy k and turbulent dissipation rate ε were calculated respectively by the following equations

$$\frac{\partial}{\partial t}(\alpha_q \rho_q k_q) + \nabla \cdot (\alpha_q \rho_q \vec{v}_q k_q) = \\ = \nabla \cdot \left(\alpha_q \frac{\mu_{t,q}}{\sigma_k} \nabla k_q \right) + \alpha_q G_{k,q} - \alpha_q \rho_q \varepsilon_q + \alpha_q \rho_q \Pi_{k_q} \tag{9}$$

$$\frac{\partial}{\partial t}(\alpha_q \rho_q \varepsilon_q) + \nabla \cdot (\alpha_q \rho_q \vec{v}_q \varepsilon_q) = \\ = \nabla \cdot \left(\alpha_q \frac{\mu_{t,q}}{\sigma_\varepsilon} \nabla \varepsilon_q \right) + \\ + \alpha_q \frac{\varepsilon_q}{k_q} (C_{1\varepsilon} G_{k,q} - C_{2\varepsilon} \rho_q \varepsilon_q) + \alpha_q \rho_q \Pi_{\varepsilon_q} \tag{10}$$

Where, $\sigma_k = 1.0$, $\sigma_\varepsilon = 1.3$, $C_{1\varepsilon} = 1.44$, $C_{2\varepsilon} = 1.92$, $C_\mu = 0.09$were chosen as model constants. The dispersed turbulence model was used to model the turbulence of dispersed phase (gas bubble).

In this simulation, the bubble size was assumed constant. The mean diameter d of bubbles was set at 4 mm according to Li's experimental observation.[18]

Model validation

Since the ratio of reactor length to width is 5, the effects of side walls on the flow velocity in the direction of length are generally small. To reduce the computation load, a 40 mm thick sliver along the length of the reactor was selected as the computation domain, where the two side interfaces were set as periodic boundaries. The standard wall functions and no-slip conditions were applied on the wall. The free surface of the reactor was considered as pressure outlet boundary condition. At the tube sparger, zero velocity for liquid and special gas vertical velocity calculated from aeration rate were given as the inlet boundary condition. The initial condition was zero liquid velocity and gas volume fraction in the bioreactor.

At the inlet boundary, the size function was used to make the mesh refinement to guarantee the requirement of computational precision. The unstructured tetrahedral meshes were adopted in the flow field mesh division. The computational grids are shown in Fig. 1(b).

To gain the mesh size-independent solution, three cases of grids including large-grid (58207), middle-grid (117527) and small-grid (223036) were tested. It was found that the result of the middle-grid was close to that of small-grid. Thus, the middle-grid was finally employed in all simulations.

The Phase Coupled SIMPLE algorithm was adopted to couple the interaction of the phases. The first order upstream scheme was applied for obtaining the algebraic equations of momentum, volume fraction, turbulent kinetic energy and dissipation rate. The convergence criteria adopted in all simulations was 1×10^{-4}. After the initial flow field was assumed, the steady-state flow field was calculated by unsteady simulation. The steady state flow was obtained if the export gas flow rate was equal to the import flow rate. In addition, the monitor values of liquid velocity from three equidistant cross-sections along the y-axis direction did not change.

The experimental results of Li[18] were adopted to verify the correctness of the simulation. Fig. 2 shows the average gas holdup (α_p) and the mean liquid velocities in the riser and downcomer under different aeration rates. The aeration rate is the ratio of the gas volume injected into the reactor in one-minute to the liquid volume. It was found that the simulation results agreed well with the related experiments and the maximum relative error was less than 10 %.

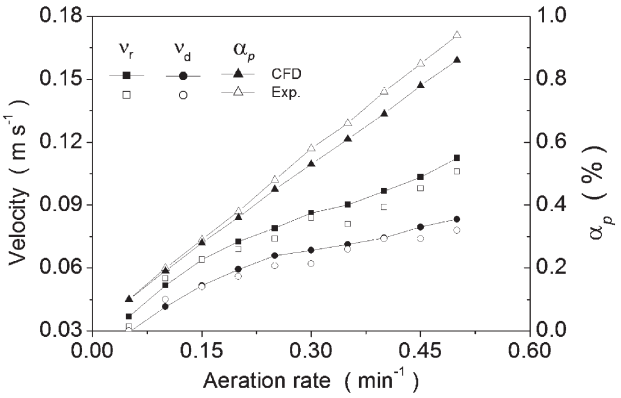

Fig. 2 – *Comparison of simulation data with related experimental data from Li*[18]

The choice of operation and evaluation parameters

The downcomer is the main photosynthesis zone for PBR and a lager downcomer space is favorable to algae growth. The optimal reactor structure parameters $A_d/A_r = 1.62$, a = 260 mm, b = 20 mm were obtained in Li's study[18]. However, the volume ratio of downcomer to the whole reactor was only 26 %. Besides, under the structure of a = 260 mm and b = 20 mm, the size of waved baffles is too small to make a sufficient study of the wave baffle structure: L/λ and A/λ. Therefore, it

was necessary to enlarge the downcomer space. As A_d/A_r was constant, changing the structure parameters of a and b shown in Fig. 1 mainly influenced the mass transfer performance.[16,18] Thus, in this study, the inner structure parameters a = 120 mm, b = 40 mm, A_d/A_r = 1.62 were set to enlarge the downcomer zone and wave baffle size. In previous study of the downcomer mixing characteristic, parameters such as average turbulence kinetic energy in the downcomer ($(TKE)_d$),average liquid radial velocity in the downcomer (U_d) were used to evaluate the mixing performance.[16,23] Consequently, $(TKE)_d$ and U_d were also selected to study the effects of waved baffles on the performance of mixing in the downcomer.

Results and Discussion

Effects of waved baffles

There is a one-to-one relationship between wavelength (λ) and the number of waves. As the parameters of a and b were fixed, the waved baffle height (L) was constant. The change of L/λ will only cause change in wavelength. Therefore, under the condition of fixed wave amplitude (A) and aeration rate of 0.15, a study of the effect of L/λ on $(TKE)_d$ and U_d was carried out.

Fig. 3 describes the effect of L/λ on the mean liquid velocity in the downcomer (v_d). It is shown that v_d decreases as L/λ increases. This is because, as L/λ increases, the number of waves also increases. The resistances of waved baffles increase and result in the decrease of the liquid circulation velocity as the air velocity is constant.

Fig. 4 shows the effect of L/λ on $(TKE)_d$. It is found that $(TKE)_d$ decreases with the increase of L/λ and tends to be constant as L/λ increased from 7 to 10. When L/λ is beyond 10, the value of $(TKE)_d$ fluctuates. It has a minimum value as L/λ is 11 and

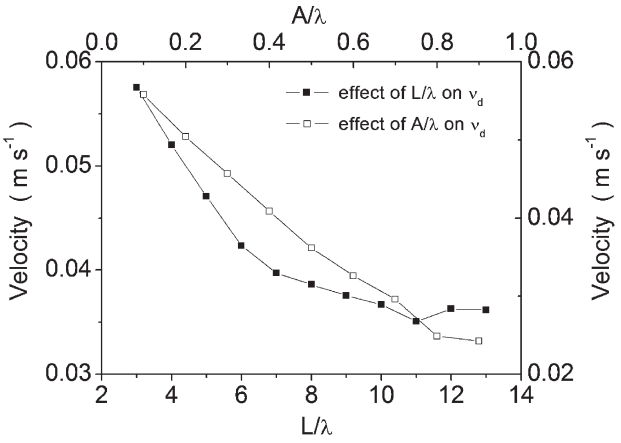

Fig. 3 – *Effects of L/λ and A/λ on v_d*

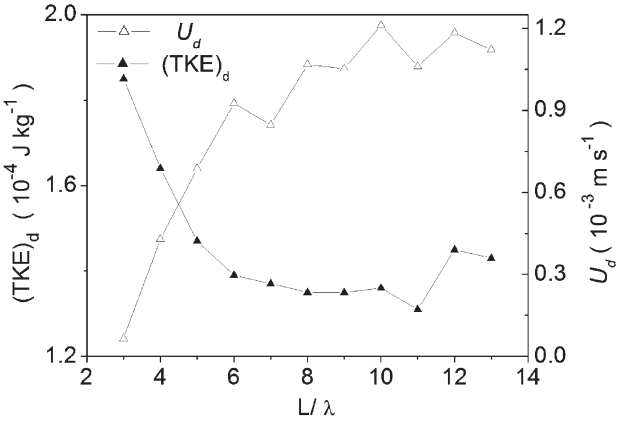

Fig. 4 – *Effects of L/λ on $(TKE)_d$ and U_d*

a larger value as L/λ is 12. The change trend of $(TKE)_d$ is similar to that of v_d. This is because the factors that can bring changes in $(TKE)_d$ include liquid velocity, number of waves and the dead zone. When L/λ increases, the number of waves also increases, which helps to increase the chance of turbulent mixing. But because the mean liquid velocity itself is small and becomes smaller with the increase of L/λ, it is hard to make an efficient turbulent mixing under the weak liquid velocity. Thus $(TKE)_d$ decreases with the decrease of v_d. It is also found that v_d has a major influence on $(TKE)_d$. There is the same change trend between $(TKE)_d$ and v_d.

Fig. 4 shows the effect of L/λ on U_d. It is found that U_d increases as L/λ increases from 3 to 6. When L/λ is beyond 6, U_d fluctuates at a high value level. The reason is that when L/λ is below 6, v_d is large and the liquid mainly circulates in y-axis direction. The value of U_d is small. As L/λ increases, the number of waves and wave peaks also increases. The turbulent mixing near the wave peak was enhanced which led to an increase in U_d. When L/λ is beyond 6, on one hand, the increase of L/λ decreases the liquid velocity which includes velocities in both x-axis and y-axis directions. On the other hand, the turbulent mixing was enhanced with the increase of the number of waves. Increasing L/λ is helpful to raise the frequency of turbulence mixing. Thus, the gradually declining liquid velocity together with the increasing frequency of turbulence mixing, results in the fluctuation of U_d.

The change of L/λ has a great influence on light-gradient mixing process represented by the parameters U_d and $(TKE)_d$. When L/λ is 12, the values of U_d and $(TKE)_d$ are at a high level, which is suitable for creating good light-gradient mixing conditions. Therefore, L/λ was chosen as 12 and the position of the central axis of waved baffle (h) in the reactor was fixed. Under these conditions, the effect of A/λ on the light-gradient mixing was stud-

ied. As L/λ is 12, L and λ are constant. The change of A/λ will only change the parameter of A.

Fig. 3 shows the effect of A/λ on the mean liquid velocity in the downcomer. It is found that v_d decreases as A/λ increases. This may be explained that under a given gas velocity, the flow resistance increases because of the increase of A/λ. The liquid circulation velocity decreases. Thus, v_d also decreases gradually as A/λ increases.

The effects of A/λ on $(TKE)_d$ are shown in Fig. 5. As A/λ is below 0.3, $(TKE)_d$ increases gradually with the increase of A/λ. When A/λ is beyond 0.3, $(TKE)_d$ decreases as A/λ increases. This is because when A/λ is 0.1, the wave amplitude is small, it is hard to make effective turbulent mixing, so the value of $(TKE)_d$ is small. As A/λ increases from 0.1 to 0.3, wave amplitude increases. Under the aid of wave baffles, the turbulent mixing is enhanced. The value of $(TKE)_d$ becomes large. However, because the liquid velocity decreases with the increase of A/λ, the increase extent of $(TKE)_d$ weakens. As A/λ is 0.3, the value of $(TKE)_d$ reaches the largest value. With the increase of A/λ, the liquid velocity decreases gradually, which leads to a weak turbulent mixing. Besides, the zone of the adjacent wave peak in the same waved baffle increases and the dead zone of the adjacent wave peak also gradually increases with the increase of A/λ. As a result, $(TKE)_d$ decreases gradually.

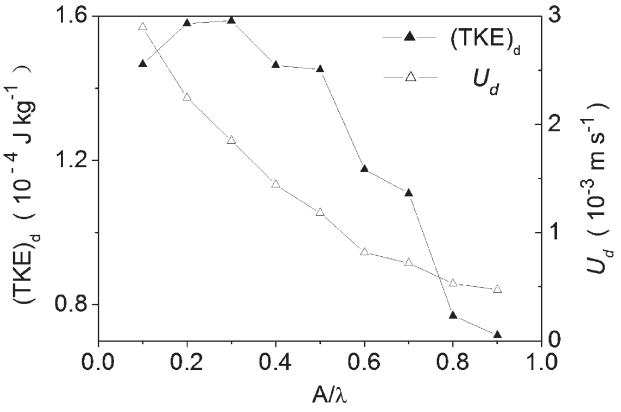

Fig. 5 – *Effects of A/λ on $(TKE)_d$ and U_d*

The effect of A/λ on U_d is shown in Fig. 5. It can be seen that U_d decreases gradually with the increase of A/λ. This can be understood that the clearance between the two adjacent wave peaks at the same waved baffle is small and the mean liquid velocity is relatively large for the small A/λ, because of which a good mixing performance near the wave peak can be obtain. The value of U_d is larger. However, when A/λ increases, the liquid velocity decreases gradually, which leads to a weak turbulent mixing. Besides, the zone of the adjacent wave peak in the same waved baffle increases and the dead zone of the adjacent wave peak also gradually increases with the increase of A/λ, because of which U_d decreases gradually.

Evaluation of waved baffles

It was found that as L/λ was 12, the values of U_d and $(TKE)_d$ were large under the given aeration rate of 0.15 and wave amplitude. Under this condition, as A/λ was 0.2, large values of $(TKE)_d$ and U_d were obtained, which is advantageous to create a good mixing in the irradiation direction. Thus, the optimized structure of waved baffle is that $L/\lambda = 12$ and $A/\lambda = 0.2$, under which better performance of light-gradient mixing was obtained.

In order to evaluate the light-gradient mixing performance under the condition of the optimized waved baffles, traditional flat baffles were established. The same structure parameters ($A_d/A_r = 1.62$, a = 260 mm, b = 40 mm) and simulation conditions were made. The comparison results between the flat baffles and the optimized waved baffles are shown in Table 1.

Table 1 – *Simulation results of different guide plate structures*

Type	L/λ	A/λ	v_d [m s^{-1}]	U_d [m s^{-1}]	$(TKE)_d$ [J kg^{-1}]
Flat baffles	–	–	5.74E-2	4.31E-3	1.17E-4
Waved baffles	12	0.2	5.04E-2	2.25E-3	1.58E-4

The results show that for the optimized waved baffle, the value of $(TKE)_d$ increases about 35 % compared with that of flat baffles. This is because the effective turbulence mixing in the downcomer is hard to create under the action of flat baffles while it is possible in the optimized waved baffles. Therefore, there is great increase in $(TKE)_d$ under the action of optimized waved baffles. Lin et al.[23] found that the higher the value of $(TKE)_d$ was, the better mixing in the downcomer and the *Isochrysis galbana* 3011 growth. For flat-baffles, the value of U_d is much higher than that of waved baffles, the reason may be that without the resistance in liquid flow direction in the flat baffles case, the liquid velocity in the downcomer is larger than that of waved baffles case. Although the radial mixing is weak under the action of flat baffles, the liquid radial velocity created by liquid normal flow is large because of the higher liquid velocity. Therefore, U_d is much higher in the flat baffles case than that of waved baffles.

Algal photosynthesis mainly takes place in the downcomer, and the accuracy of control parameters obtained from the CFD simulation makes sense for

the optimization of reactor. Previous studies mainly employed mean values of the relevant parameters as evaluation indicators.[16, 23] But the mean value cannot reflect the value distribution character of related parameters. A statistical approach was applied here to analyze the value distribution of turbulent mixing parameters in the downcomer. The flat baffles and the optimized waved baffles presented in Table 1 were studied. Because the flow field is uniform in the length direction of the reactor, the hydrodynamic behaviors of two symmetrical downcomers are the same. Five equidistant cross-sections along the z-axis direction in one-side downcomer were chosen. The turbulence kinetic energy and liquid radial velocity of each grid located in these cross-sections were analyzed.

The distributions of liquid radial velocity in both waved baffles and flat baffles are shown in Fig. 6. Because of the lack of resistance in liquid circulation, the maximum liquid radial velocity in the downcomer from flat baffles is higher than that of waved baffles, this is why U_d obtained from flat baffles is larger than that of waved baffles. Although the maximum liquid radial velocity in the downcomer from flat baffles is large, its proportion is very low. Therefore, the average liquid radial velocity cannot reflect the real radial mixing condition exactly. Besides, it is found that the proportion of the negative liquid velocity is 11.38 % in the reactor with waved baffles, while it is only 4.54 % in the reactor with flat baffles. The large proportion of negative velocity indicates that a large space is occupied by turbulence eddy. In the optimized waved baffles, the proportion of the negative liquid velocity is 2.5 times that of flat baffles. Therefore, turbulent mixing is well improved in the PBR with optimized waved baffles.

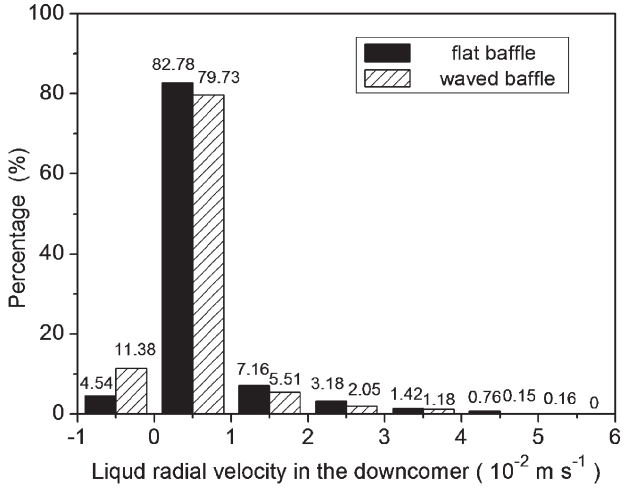

F i g . 6 – *Distribution percentage of liquid radial velocity in the downcomer of the flat plate PBR with waved baffles and flat baffles*

The distributions of turbulence kinetic energy in the downcomer of the reactor with waved baffles and flat baffles are shown in Fig. 7. It is found that the maximum value of turbulence kinetic energy in the downcomer in the reactors with waved baffles is higher than that with flat baffles. This is because the turbulent perturbation is enhanced under the action of waved baffles. The large turbulence kinetic energy is gained by high intensity turbulence. For the optimized waved baffles, the value of $(TKE)_d$ is 1.58E–4 J/kg. The percentages of turbulence kinetic energy in the downcomer that are larger than the mean value are 36.6 % and 19.1 % in the reactors with waved baffles and flat baffles, respectively. The larger distribution percentage of turbulence kinetic energy in the downcomer in reactor with optimized waved baffles means a better mixing performance.

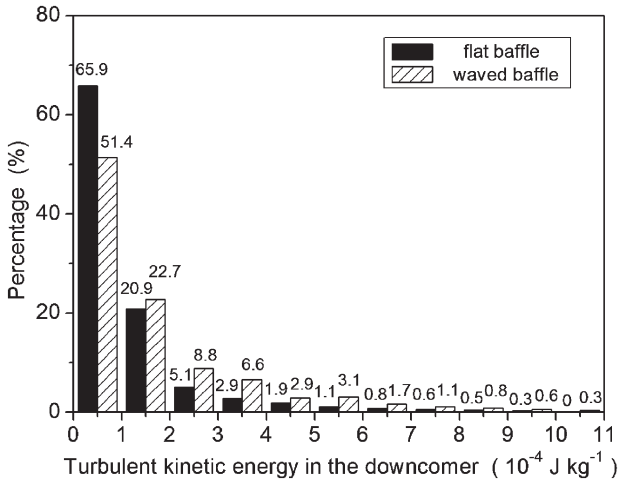

F i g . 7 – *Distribution percentage of turbulence kinetic energy in the downcomer of the flat plate PBR with waved baffles and flat baffles*

For better intuitive appreciation of the mixing performance, the streamlines of bioreactors with optimized waved baffles, flat baffles and the special waved baffles of bad mixing performance were investigated. Two-dimensional pictures of streamlines were given in order to make a clear observation and comparison. It can be seen from Fig. 8 (A) that a good mixing performance was created under the action of optimized waved baffles. The liquid waved regularly in the flow field, which made algae experience fluctuations along the light irradiation. The flow field characteristic is similar to the liquid flow with sinusoidal variation created by a helical static mixer in Perner-Nochta's research. In his research, the liquid exchange could not only improve the radial liquid exchange with a high, well defined, frequency, but also increase the light yield on the microscopic scale and therefore enhance algal

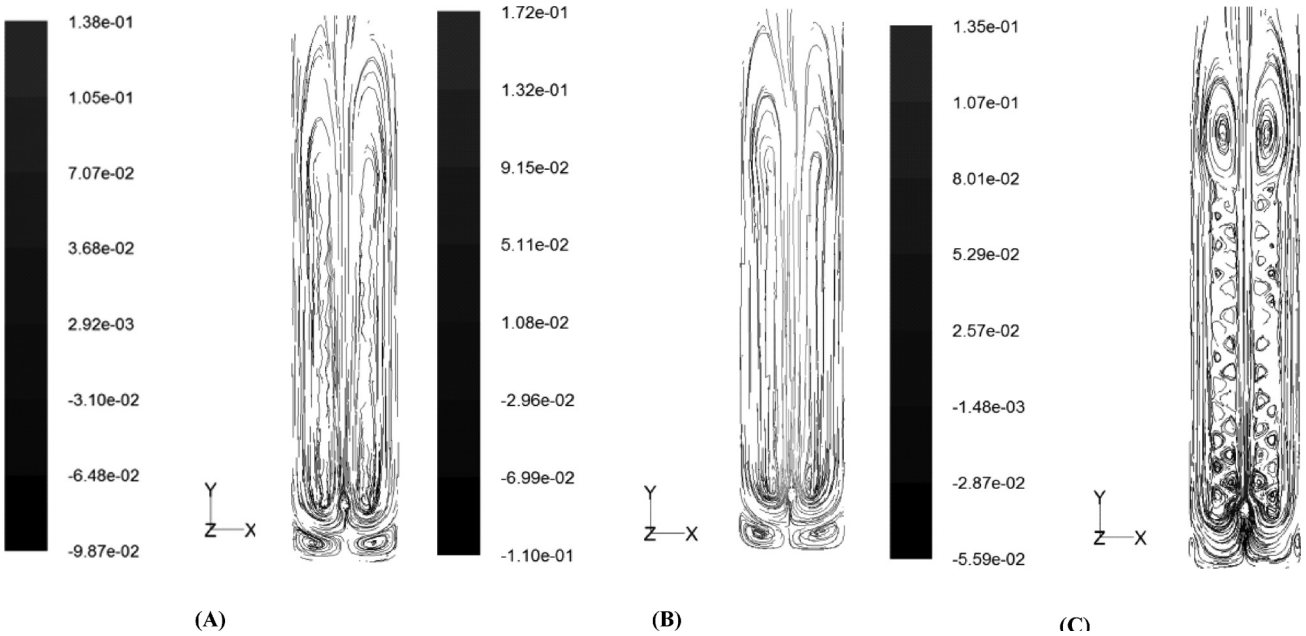

F i g . 8 – *Streamlines of three different baffles: (A) optimized waved baffles with structures of L/λ = 12 and A/λ = 0.2; (B) flat baffles; (C) waved baffles with structures of L/λ = 12 and A/λ = 0.2.*

growth.[14] In Fig. 8 (B), liquid velocity of the flat baffles case is larger than that of optimized waved baffles, since there is less resistance of wave wall along the liquid flow direction. However, the liquid mainly flows along y-axis direction and the radial mixing is very weak. Therefore, the light-gradient mixing was enhanced under the action of optimized waved baffles compared with that of flat baffles case. In addition, the streamline of waved baffles with the structure of L/λ = 12 and A/λ = 0.9 was also investigated. As shown in Fig. 8 (C), the dead zones appear near the two adjacent wave peaks at the same waved baffle. Besides, the local vortexes also appear in the same zone and greatly limit material exchange process and microalgae growth. The effective light-mixing is hard to achieve because of those dead zones and low liquid velocity values, which may be an explanation why both $(TKE)_d$ and U_d are small in Fig. 5.

Conclusions

Three-dimensional and two-fluid CFD simulation of a flat plate photobioreactor with waved baffles has been performed. The effects of waved baffles structure parameters: the ratio of waved baffle height to wave length (L/λ) and the ratio of wave amplitude to wave length (A/λ) on light-gradient mixing was investigated. It was shown that waved baffles could effectively regulate the light-gradient mixing process. The optimized waved baffles structure parameters of L/λ = 12 and A/λ = 0.2 was obtained, under which both the average liquid radial velocity and average turbulent kinetic energy in the downcomer were large. A good performance of light-gradient mixing was created. Under this condition, the value of average turbulence kinetic energy in the downcomer increased by 35 % compared with that of traditional flat baffles. The proportion of the negative liquid velocity, which can indicate the radial mixing condition, is about 2.5 times larger than that of flat baffles. Evaluation results and statistic analysis indicated that optimized waved baffles could greatly improve light-gradient mixing compared with traditional flat-baffles.

Symbols used

A – wave amplitude, m
C_D – drag coefficient, –
D_q – liquid-phase diffusion coefficient, $m^2\ s^{-1}$
d – bubble diameter, mm
$F_{i,p}$ – force exerted on gas, N
$F_{i,q}$ – force exerted on liquid, N
$\overline{F}$ – interphase force, N
h – the central axis of the waved baffle, –
G_k – turbulence generation term, kg $m^{-1}\ s^{-3}$
g – gravitational acceleration, m s^{-2}
k – turbulent kinetic energy, $m^2\ s^{-2}$
K – interphase momentum transfer coefficient, kg $m^{-3}\ s^{-1}$
k_La – liquid-phase volumetric mass transfer coefficient, s^{-1}
L – waved baffle height, m
m_q – the mass of q phase, kg
m_{pq} – the mass transfer from p phase to q phase, kg

p – pressure, Pa

Re – Reynolds number, –

v_r – mean liquid velocity in the riser, m s^{-1}

v_d – mean liquid velocity in the downcomer, m s^{-1}

$\vec{v}_q$ – liquid velocity vector, m s^{-1}

$\vec{v}_p$ – gas velocity vector, m s^{-1}

$\vec{v}_{i,p}$ – gas velocity component, m s^{-1}

$\vec{v}_{i,q}$ – liquid velocity component, m s^{-1}

U_d – average liquid radial velocity in the downcomer, m s^{-1}

t – time, s

$(TKE)_d$ – average turbulence kinetic energy in the downcomers, J kg^{-1}

Greek symbols

α – phase volume fraction, –

ε – turbulent energy dissipation rate, m^2 s^{-3}

$\bar{\bar{\tau}}_q$ – stress-strain tensor, –

ρ – fluid density, kg m^{-3}

σ_k – turbulent Prandtl number for the kinetic energy, –

σ_ε – turbulent Prandtl number for the rate of dissipation of energy, –

μ – shear viscosity, kg m^{-1} s^{-1}

$\mu_{t,q}$ – liquid phase turbulent viscosity, pa s

λ – wavelength, m

Superscripts and subscripts

i – coordinate variable

p – gas phase

q – liquid phase

References

1. *Spolaore, P., Joannis, C., Duran, E. et al*., J. Biosci. Bioeng. **101** (2006) 87
2. *Wijffels, R. H., Barbosa, M. J*., Science **329** (2010) 796
3. *Mata, T. M., Martins, A. A., Caetano, N. S*., Renew. Sust. Energ. Rev. **14** (2010) 217
4. *Milledge, J. J*., Rev. Envion. Sci. Biotechnol. **10** (2011) 31
5. *Borowitzka, M. A*., J. Biotechnol. **70** (1999) 313
6. *Ulrike, S. S., Renate, P., Peter, M. et al*., Chem. Ing. Tech. **81** (2009) 1783
7. *Suh, I. S., Lee, C. G*., Biotechnol. Bioproc. E. **8** (2003) 313
8. *Clemens, P.*, Eng. Life. Sci. **9** (2009) 165
9. *Janssen, M., Tramper, J., Mur, L. R. et al*., Biotechnol. Bioeng. **81** (2003) 193
10. *Xu, L., Weathers, P. J., Xiong, X. R. et al*., Eng. Life. Sci. **9** (2009) 178
11. *Kunjapur, A. M., Eldridge, R. B*., Ind. Eng. Chem. Res. **49** (2010) 3516
12. *Yoshimoto, N., Sato, T., Kondo, Y*., J. Appl. Phycol. **17** (2005) 207
13. *Richmond, A*., Hydrobiologia **512** (2004) 33
14. *Perner-Nachta, I., Posten, C*., J. Biotechnol. **131** (2007) 276
15. *Su, Z., Kang, R., Shi, S. et al*., Biomass Bioenergy **34** (2010) 1879
16. *Yu, G., Li, Y., Shen, G. et al*., J. Appl. Phycol. **21** (2009) 719
17. *Degen, J., Uebele, A., Retze, A. et al*., J. Biotechnol. **92** (2001) 89
18. *Li, Y., Qi, X., Liu, T. et al*., Chin. J. Proc. Eng. **10** (2010) 849
19. *Simcik, M., Mota, A., Ruzicka, M. C. et al*., Chem. Eng. Sci. **66** (2011) 3268
20. *Tabib, M. V., Roy, S. A., Joshi, J. B*., Chem. Eng. J. **139** (2008) 589
21. *Mao, Z. S*., Chin. J. Proc. Eng. **8** (2008) 645
22. *Huang, Q., Yang, C., Yu, G. et al*., Chem. Eng. Technol. **30** (2007) 870
23. *Lin, C., Li, Y., Wang, W. et al*., J. Chem. Eng. Chin. Univer. **23** (2009) 263